Theoretical Study on the Spectroscopic Parameters and Transition Properties of MgH Radical Including Spin–orbit Coupling *

Dong-Lan Wu(伍冬兰)[1,2], Bin Tan(谭彬)[1], Xue-Feng Zeng(曾学锋)[1], Hui-Jun Wan(万慧军)[1], An-Dong Xie(谢安东)[1], Bing Yan(闫冰)[2**], Da-Jun Ding(丁大军)[2**]

[1] *College of Mathematic and Physical, Jinggangshan University, Ji'an 343009*
[2] *Institute of Atomic and Molecular Physics, Jilin University, Changchun 130012*

(Received 15 April 2016)

An accurate theoretical study on the MgH radical is reported by adopting the high-level relativistic MRCI+Q method with a quintuple-zeta quality basis set. The reliable potential energy curves of the five Λ-S states of MgH are derived. Then the associated spectroscopic parameters are determined and found to be in good accordance with the available experimental results. The permanent dipole moments (PDMs) and the spin–orbit (SO) matrix elements of Λ-S states are computed. The results show that the abrupt changes of PDMs and SO matrix elements are attributed to the variations of electronic configurations at the avoided crossing point. The SOC effect leads to the five Λ-S states split into ten Ω states and results in the double potential well of (2)1/2 state. Finally, the transition properties from the (2)1/2, (1)3/2 and (3)1/2 states to the ground state $X^2\Sigma+1/2$ transitions are obtained, including the transition dipole moments, Franck–Condon factors and radiative lifetimes.

PACS: 31.50.Df, 31.50.Bc, 31.15.aj DOI: 10.1088/0256-307X/33/6/063102

MgH has become an important molecule in astrophysics due to the fact that its visible bands appear strongly in the absorption spectra of the sun and some cool stars.[1–3] It is used routinely to estimate the magnesium isotope abundances.[4,5] The first series of spectroscopic studies on MgH were carried out in the 1920s and 1930s, shortly after the development of quantum mechanics, and several electronic transitions involving the ground electronic state $X^2\Sigma^+$ and the low-lying excited states were observed and analyzed.[6–9]

In experiment, Barclay *et al.*[10] and Shayesteh *et al.*[11] studied the vibrational transitions of the $X^2\Sigma^+$ state. There are many experimentally measured spectral lines for the $A^2\Pi$–$X^2\Sigma^+$ and $B'^2\Sigma^+$–$X^2\Sigma^+$ transitions,[12–14] although the $X^2\Sigma^+$ state transitions have only been observed in the infrared up to $\nu = 4$. The pure rotational transition with the hyperfine structure of the $X^2\Sigma^+$ state was resolved by Leopold *et al.*,[15] Lemoine *et al.*[16] and Ziurys *et al.*[10] by using a high-resolution millimetre wave. In addition, Shayesteh *et al.*[17] have provided accurate experimental information for the $A^2\Pi$ and $B'^2\Sigma^+$ excited states, i.e., the Dunham-type constants and the Rydberg–Klein–Rees (RKR) potential curves.

In addition to the experimental works mentioned above, there are some theoretical calculations for the $X^2\Sigma^+$, $A^2\Pi$ and $B'^2\Sigma^+$ states. The potential energy curves (PECs) and dipole moment curves (DMCs) of MgH by Saxon *et al.*[18] were made with an important contribution to theoretical development of this molecule. Kirby *et al.* published a series of works[19–21] on theoretical line lists and line intensities of MgH, who made use of Saxon's ab initio PECs and DMCs for the $X^2\Sigma^+$, $A^2\Pi$ and $B'^2\Sigma^+$ states.[18] Unsurprisingly, their results have substantial discrepancies with the available experimental data.[11,13,17] Since the DMCs were computed by Saxon *et al.*[18] more than thirty years ago, no more accurate works can be combined with the experimental potential curves. The most accurate way to calculate radiative lifetimes and the Einstein coefficients is to combine experimental potential curves and energy levels with ab initio transition dipole moments. Although two theoretical studies on the low-lying states of MgH have been published very recently,[22,23] neither of them included transition dipole moments. Since then, Mostafanejad *et al.* calculated the potential curves and transition dipole moments,[24] but they did not take into consideration the core-valence correlation and scalar relativistic influence. In particular, the spin-orbit coupling (SOC) effect, which may play an important role in the spectroscopic and dynamic characteristics of electronic states, was not considered in the previous works. For these reasons, we carry out accurate theoretical calculations on the low-lying excited states of MgH using a high-level ab initio method MRCI+Q with consideration of core-valence correlation, scalar relativistic effect and SOC effect.

In this Letter, all of the calculations have been performed by the quantum chemistry MOLPRO 2012 program package.[25] The spectroscopic constants and transition properties are obtained with the LEVEL 8.0 program.[26] Owing to the limitation of the MOLPRO program, C_{2v} point group symmetry, which is the Abelian subgroup of $C_{\infty v}$, is adopted in the calculations. For MgH, $3a_1$, $1b_1$ and $1b_2$, symmetry molecular orbitals (MOs) are determined as the active space, which correspond to the atomic Mg $3s3p$ and H $1s$ shells. The outermost Mg $3s^2$ and H $1s^1$ electrons are placed in the active space. The 8 electrons of the $2s^22p^6$ shell for Mg are placed in the closed shell.

*Supported by the National Natural Science Foundation of China under Grant Nos 11564019, 11574114, 11147158, 91221301and 11264020, and the Natural Science Foundation of Jilin Province under Grant No 20150101003JC.
**Corresponding author. Email: yanbing@jlu.edu.cn; dajund@jlu.edu.cn
© 2016 Chinese Physical Society and IOP Publishing Ltd

Furthermore, these orbitals are doubly occupied in all reference configuration state functions, and correlated via single and double excitations. In these calculations of electronic structure and single-point energy, we choose the contracted all-electron augmented correlation consistent basis sets aug-cc-pwCV5Z-DK[27] for Mg and aug-cc-pV5Z-DK[28] for H, respectively.

To obtain the high-precision PECs of MgH, the single-point energies are calculated by using the restricted Hartree–Fock (RHF) self-consistent field (SCF) method first. Then the multi-configuration wave function is constructed by the state-averaged complete active space SCF (SA-CASSCF) method.[29,30] Finally, the internally contracted multi-reference configuration interaction (ic-MRCI) approach[31,32] plus Davidson correction (+Q) is employed to obtain the correlation energy calculation and achieve the accurate energies. At the same time, the relativistic effect is treated with the one-electron integral third-order Douglas–Kroll integrals.[33] The SOC effect is taken into consideration at the CASSCF level via the state interaction approach.[34]

With the aid of the PECs of the Λ-S and Ω electronic states, the spectroscopic constants, including equilibrium internuclear distance R_e, excitation energy T_e, vibrational constants ω_e and $\omega_e\chi_e$, balanced rotation constant B_e, and vibration–rotation coupling constant α_e are determined by numerical solution of the one-dimensional nuclear Schrödinger equation. The dissociation energy D_e is obtained by subtracting the molecular energy at R_e from the energy at a large separation. The TDMs and the permanent dipole moments are evaluated at the ic-MRCI level. The FCFs are calculated with the LEVEL program. The radiative lifetimes of the several lowest transitions are predicted based on the TDMs and FCFs lastly.

Table 1. The spectroscopic constants of the Λ-S states.

Λ-S state		T_e (cm^{-1})	R_e (Å)	ω_e (cm^{-1})	$\omega_e\chi_e$ (cm^{-1})	B_e (cm^{-1})	α_e (cm^{-1})	D_e (eV)	Configuration at R_e (%)
$X^2\Sigma^+$	This work	0.0	1.732	1491.98	30.248	5.812	0.2434	1.3840	$4\sigma^25\sigma^16\sigma^02\pi^0$(86)
	Calc.[24]	0.0	1.741	1491.6	31	-	-	1.4268	$4\sigma^25\sigma^06\sigma^12\pi^0$(6.2)
	Calc.[18]	0.0	1.743	1484.4	31	5.7177	0.1453	1.3844	
	Calc.[22]	0.0	1.72	1453.7	29.4	-	-	1.3608	
	Calc.[23]	0.0	1.726	1494.68	34.25	5.7817	0.1764	1.4037	
	Expt.[17]	0.0	1.729682	1492.776	29.84	-	-	1.3762	
	Expt.[34]	0.0	1.7297	1495.20	7 31.889	5.8257	0.1859	1.3768	
$A^2\Pi$	This work	19182.2081	1.6825	1608.0984	31.3209	6.1628	0.2619	1.6981	$4\sigma^25\sigma^06\sigma^02\pi^1$(88)
	Calc.[24]	18924	1.693	1581.5	34.4	-	-	1.6733	$4\sigma^15\sigma^16\sigma^02\pi^1$(3.8)
	Calc.[18]	19172	1.699	1561.8	33.2	6.0373	0.1768	1.6033	$4\sigma^05\sigma^26\sigma^02\pi^1$(3.2)
	Calc.[22]	19397	1.67	1551.3	31.2	-	-	1.6425	
	Calc.[23]	18893	1.693	1580.8	30.2	-	-	1.6868	
	Expt.[17]	19225.534	1.67827	1600.334	31.870	-	-	1.7040	
	Expt.[34]	19226.8	1.6778	1598.17	31.085	6.1913	0.1931	1.4369	
$B'^2\Sigma^+$	This work	22421.9782	2.5525	829.5202	11.4192	2.6782	0.0099	1.3091	$4\sigma^15\sigma^26\sigma^02\pi^0$(64)
	Calc.[24]	22214	2.635	816.7	11.7	-	-	1.2678	$4\sigma^25\sigma^06\sigma^12\pi^0$(22)
	Calc.[18]	22035	2.622	818.6	13.1	2.5320	0.018	1.2455	$4\sigma^15\sigma^06\sigma^02\pi^2$(2.8)
	Calc.[22]	22051	2.59	831.5	12.3	-	-	1.3122	$4\sigma^25\sigma^16\sigma^02\pi^0$(2.4)
	Calc.[23]	22250	2.634	816.7	12.1	-	-	1.2709	
	Expt.[17]	22410.190	2.59404	828.324	11.477	-	-	1.3069	
	Expt.[34]	22410.5	2.597	828.0	11.6	2.596	-	1.3904	

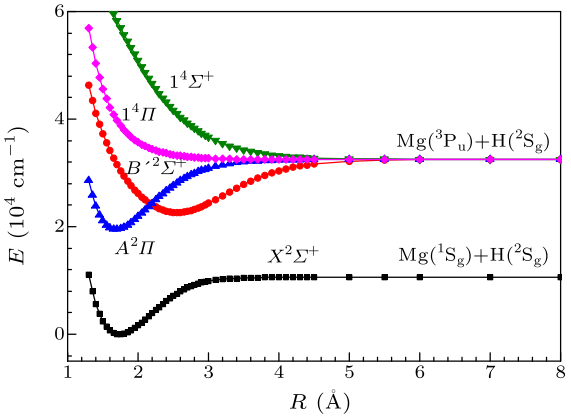

Fig. 1. The PECs of the Λ-S states.

The five Λ-S states including $X^2\Sigma^+$, $A^2\Pi$, $B^2\Sigma^+$, $1^4\Pi$, and $1^4\Sigma^+$, which are correlated with the two lowest dissociation limits of Mg(^1S_g)+H(^2S_g) and Mg(^3P_u)+H(^2S_g), were studied by using the MRCI+Q method with aug-cc-pwCV5Z-DK for Mg and aug-cc-pV5Z-DK for H, respectively. The selected step lengths were 0.05 Å for R =1.3–3.0 Å and 0.1 Å for R =3.0–8.0 Å in the calculations of single point energy for these states. The calculated PECs of the five Λ-S states are plotted in Fig. 1. As shown in Fig. 1, all the Λ-S states are dissociated into neutral Mg and H atoms. The two quadruple states $1^4\Pi$ and $1^4\Sigma^+$ are typically repulsive states, while the remaining double states are bound states. Each of the $X^2\Sigma^+$, $A^2\Pi$, and $B'^2\Sigma^+$ states has a global energy minimum at the corresponding equilibrium bond distance R_e. The $A^2\Pi$ and $B'^2\Sigma^+$ states cross with each other at the bond length of about 2.16 Å.

Based on the PECs of the bound states, the corresponding spectroscopic results as well as the main electronic configuration state functions near R_e of each state are tabulated in Table 1. From Table

1, the ground state $X^2\Sigma^+$ of MgH is mainly characterized by the closed-shell electronic configuration $4\sigma^2 5\sigma^1 6\sigma^0 2\pi^0$. The PEC has a deep potential well in Fig. 1, and the well depth is calculated to be 1.3840 eV, which is closer to the latest experimental data of 1.3762 eV[17] and theoretical result of 1.3844 eV[18] than the result 1.4365ėV[35] in our former study. It may be due to the consideration of the SOC effect in this work. Compared with the most recent experimental data,[17] the calculated ω_e, and $\omega_e\chi_e$ results are only 0.796, and 0.401 cm^{-1} smaller, while the R_e value is 0.002318 Å larger. The values of B_e and α_e are consistent with the experimental data[34] by the difference of 0.0137 and 0.0575 cm^{-1}.

The first excited state $A^2\Pi$ mainly arises from the electronic configuration $4\sigma^2 5\sigma^0 6\sigma^0 2\pi^1$ corresponding to the 5σ to 2π one-electron excitation. The dissociation energy D_e is much larger than that of the ground state. The depth of the potential well is calculated to be 1.6981 eV, which is close to the recent experimental data of 1.7040 eV.[17] The values of T_e, ω_e, $\omega_e\chi_e$, B_e, α_e and R_e are 19182.2081, 1608.0984, 31.3209, 6.1628, 0.2619 cm^{-1} and 1.6825 Å, respectively, which are in good agreement with the related theoretical results of 19172, 1561.8, 33.2, 6.0373, 0.1768 cm^{-1} and 1.699 Å by using the MRCI method.[18]

The second excited state $B'^2\Sigma^+$ mainly consists of the electronic configurations $4\sigma^1 5\sigma^2 6\sigma^0 2\pi^0$ and $4\sigma^2 5\sigma^0 6\sigma^1 2\pi^0$, which correspond to the 4σ to 5σ and 5σ to 6σ excitations. Our calculated spectroscopic constants of $B'^2\Sigma^+$ state are in good accordance with the experimental data,[34] the deviation of T_e, ω_e, $\omega_e\chi_e$, B_e, and R_e are 11.7882, 1.1962, 0.0578, 0.0822 cm^{-1} and 0.04254 Å, respectively. In addition, D_e is close to the latest experimental data,[17] and the relative difference is only 0.17%.

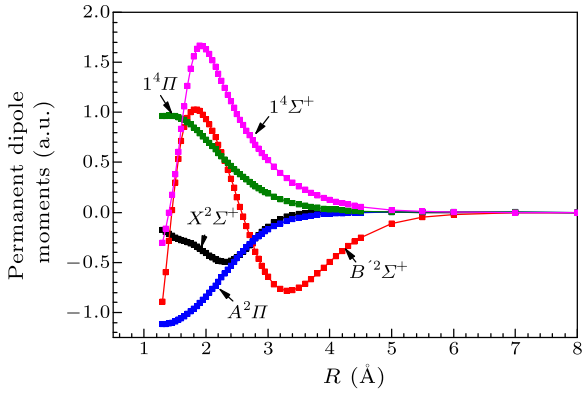

Fig. 2. The permanent dipole moments of the Λ-S states as a function of the bond distance.

The permanent dipole moments (PDMs) of the 5 Λ-S states of MgH with bond lengths are calculated and plotted in Fig. 2. The results show that the PDMs of the ground state reach 0 a.u. at the internuclear distance 3.6 Å, while the other excited states reach 0 a.u. at large distances. It could be explained that the PDMs exhibit two asymptotic limits due to the fact that the dissociation limits Mg (^1S_g)+H(^2S_g) and Mg (^3P_u)+H(^2S_g), however, all the calculated PDMs lead to consistent asymptotic limit close to 0 a.u. due to the center of positive charges with the position vector $|\lambda| \approx 0$, which is corresponding to the dissociation limit of Mg+H. In addition, the PDMs of the $A^2\Pi$ and $B'^2\Sigma^+$ exhibit a pair of leaps at the avoided crossing region of the two states due to the change of the wave functions. The similar cases of PDMs are also observed in MgX radical,[36] ZnH^+[37] and CdH^+ cations.[38]

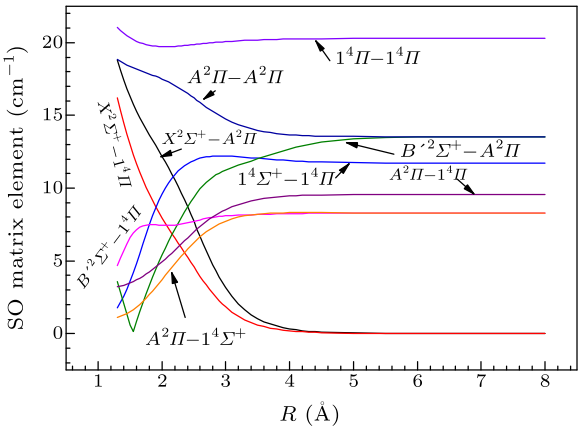

Fig. 3. The absolute R-dependent SO matrix elements of the Λ-S states.

It is generally known that the SOC effect leads to the strong interaction between the adjacent Λ-S states and causes different Λ-S states that have common Ω states to recombine[39,40] at the intersections of PECs. To further illuminate the influence of SOC effect on the Λ-S states of MgH, the non-vanishing SOC matrix elements between $A^2\Pi$, $1^4\Pi$ and other states were calculated. As shown in Fig. 3, the SOC matrix elements involving the $A^2\Pi$ state change quickly at $R < 2.65$ Å while they vary slightly in the internuclear distance range of 2.65–5.25 Å, and finally, remain unchanged to be 5.25–8.0 Å. For instance, the $B'^2\Sigma^+$–$A^2\Pi$ coupling first decreases from 3.5 cm^{-1} at $R = 1.3$ Å to 0.2 cm^{-1} at $R = 1.5$ Å, and then increases to 13.5 cm^{-1} at $R = 8.00$ Å. This may be ascribed to the sudden change of electronic configurations of the $B'^2\Sigma^+$ state, which is mainly dominated by $4\sigma^1 5\sigma^2 6\sigma^0 2\pi^0$ and $4\sigma^2 5\sigma^0 6\sigma^1 2\pi^0$ electronic configurations at $R = 1.5$ Å, while only $4\sigma^1 5\sigma^1 6\sigma^1 2\pi^0$ configuration at $R = 8.00$ Å. It is also interesting to see the matrix elements for $1^4\Pi$-$1^4\Pi$ almost keep a constant about 20 cm^{-1}, indicating the large SOC splitting of the $1^4\Pi$ state.

For MgH radical, the original five Λ-S states split into ten Ω states after considering the SOC effect, including six $\Omega = 1/2$ states, three $\Omega = 3/2$ states, and one $\Omega = 5/2$ state. The two dissociation limits Mg(^1S_g)+H(^2S_g) and Mg(^3P_u)+H(^2S_g) split into Mg($^2S_{0g}$)+H($^2S_{1/2g}$), Mg($^3P_{0u}$)+H($^2S_{1/2g}$), Mg($^3P_{1u}$)+H($^2S_{1/2g}$), and Mg($^3P_{2u}$)+H($^2S_{1/2g}$), where Mg(^1S_g)+H(^2S_g) is associated with the singlet states of Mg($^2S_{0g}$) and H($^2S_{1/2g}$), and hence the spin–orbit splitting does not exist in the first

dissociation limit. The detailed dissociation relationships are listed in Table 2. Our calculated atomic energy intervals differ from the experimental data[41] by 0 cm^{-1}(0%), 17.505 cm^{-1}(0.08%), 17.404 cm^{-1}(0.08%) and 16.872 cm^{-1}(0.08%), respectively, indicating a fairly good agreement.

Table 2. The dissociation limits of the Ω states.

Ω state	Atomic state	Energy (cm^{-1})	
		This work	Expt.[41]
(1) 1/2	Mg($^1S_{0g}$)+H($^2S_{1/2g}$)	0	0
(2) 1/2	Mg($^3P_{0u}$)+H($^2S_{1/2g}$)	21867.91	21850.405
(3) 1/2, 1/2, 3/2	Mg($^3P_{1u}$)+H($^2S_{1/2g}$)	21887.86	21870.464
(4) 1/2, 1/2, 3/2, 3/2, 5/2	Mg($^3P_{2u}$)+H($^2S_{1/2g}$)	21928.05	21911.178

Table 3. The spectroscopic constants of the Ω states.

Ω state	T_e (cm^{-1})	R_e (Å)	ω_e (cm^{-1})	$\omega_e\chi_e$ (cm^{-1})	B_e (cm^{-1})	α_e (cm^{-1})	D_e (eV)	Dominant Λ-S composition at R_e (%)
$X^2\Sigma$+1/2	0	1.732	1491.98	30.248	5.812	0.2434	1.3840	$X^2\Sigma^+$(100)
(2)1/2$_{(int)}$	19464.2149	1.6825	1589.9737	34.8792	6.1657	0.2262	0.6264	$A^2\Pi$(100)
(2)1/2$_{(ext.)}$	22621.9701	2.5530	1157.9110	27.6983	2.6721	0.1377	1.2716	$B'^2\Sigma^+$(100)
(1)3/2	24310.4613	2.1835	1642.6369	37.7443	6.7142	0.2229	1.6987	$A^2\Pi$(99.88)
(3)1/2	19500.2793	1.6825	1196.2313	30.3955	3.1627	0.1626	1.0336	$B'^2\Sigma^+$(100)

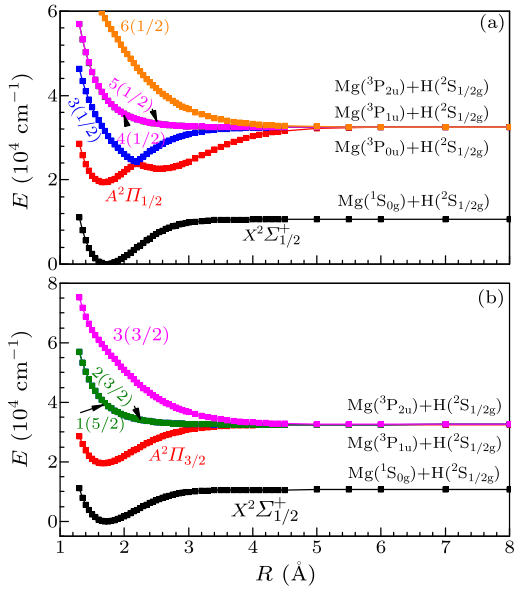

Fig. 4. The PECs of the Ω states (a) $\Omega = 1/2$ and (b) $\Omega = 3/2$ and 5/2.

The PECs of 10 Ω states are depicted in Fig. 4. As shown in Fig. 4, (4)1/2, (5)1/2, (6)1/2, (2)3/2, (3)3/2 and (1)5/2 states are pure repulsive states, which split from the two quartet repulsive $1^4\Pi$ and $1^4\Sigma^+$ states. The remaining four Ω states are bound states, which are generated from the $X^2\Sigma^+$, $A^2\Pi$ and $B'^2\Sigma^+$ states. Based on the PECs of the bound Ω states, the spectroscopic constants and their dominant Λ-S state components at R_e are all given in Table 3. From Table 3, the ground state $X^2\Sigma$+1/2 is composed of 100% $X^2\Sigma^+\Lambda$-S state. Hence, the spectroscopic constants could well reproduce the results of the Λ-S ground state $X^2\Sigma^+$. It can also be seen from Fig. 4 that there is an avoided crossing phenomenon at $R = 2.16$ Å between (2)1/2 and (3)1/2 states in Fig. 4(a), which may be the result of the SOC effect. Thus after taking the SOC effect into account, the first excited state (2)1/2 produced a double potential well, and the computed spectroscopic constants of the Ω states in Table 3 would be quite different from those for the pure Λ-S states in Table 1, especially to the dissociation energy D_e. In addition, Table 3 shows the Λ-S state compositions for the Ω=(2)1/2 state switched between the $A^2\Pi$ and $B'^2\Sigma^+$ states around $R = 2.16$ Å where the crossings occurs, strongly indicating the coupling phenomenon between the two states. We find that the potential curves of the lowest three excited states of the second dissociation limit are similar cases to H_2[42,43], which may be the similar excitation of the two molecules.

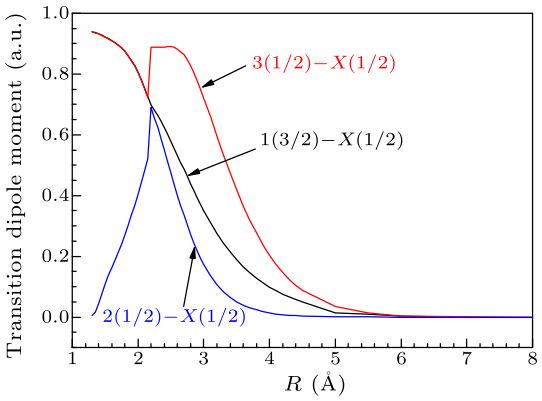

Fig. 5. The transition dipole moments of the transitions from (2)1/2, (3)1/2, and (1)3/2 to $X^2\Sigma$+1/2.

The absolute transition dipole moments (TDMs) from (2)1/2, (3)1/2, (1)3/2 to $X^2\Sigma$+1/2 state are calculated and plotted in Fig. 5. In the Franck–Condon region, the transitions of (3)1/2–$X^2\Sigma$+1/2 and (1)3/2–$X^2\Sigma$+1/2 have TDMs slightly larger than (2)1/2–$X^2\Sigma$+1/2. As illustrated in Fig. 5, the TDMs of the transition (3)1/2–$X^2\Sigma$+1/2 are characterized by a peak at the internuclear distance of 2.16 Å, where the avoided crossing between the (2)1/2 and (3)1/2 states occurs. In addition, the TDM curve of (2)1/2 increases in the beginning and then decreases to zero, which could be explained by the above-mentioned sudden change of the main Λ-S state components from the $B'^2\Sigma^+$ state to the $A^2\Pi$ state around the avoided crossing point (see Fig. 4). The present results indicate that the SOC effect plays an important role in the PECs, the spectroscopic constants as well as the transition properties of the low-lying states of MgH radical.

In view of the calculated TDMs, the radiative lifetime has been computed by[44,45]

$$\begin{aligned}\tau_{\nu'} &= (A_{\nu'})^{-1} \\ &= \frac{3h}{64\pi^4 |a_0 \cdot e \cdot \overline{TDM}|^2 \Sigma_{\nu''} q_{\nu',\nu''} (\Delta E_{\nu',\nu''})^3} \\ &= \frac{4.936 \times 10^5}{(\overline{TDM})^2 \Sigma_{\nu''} q_{\nu',\nu''} (\Delta E_{\nu',\nu''})^3},\end{aligned}$$

where ν' and ν'' symbolize the upper and lower vibrational states, $\Delta E_{\nu',\nu''}$ is the energy difference in cm^1, $q_{\nu',\nu''}$ is the FCFs, $\tau_{\nu'}$ is the radiative lifetime in seconds, and $A_{\nu'}$ is the total Einstein coefficients. The results are listed in Table 4. However, the radiative lifetime of $A^2\Pi$–$X^2\Sigma^+$ should come from the contributions of the (2)1/2–$X^2\Sigma$+1/2 and (1)3/2–$X^2\Sigma$+1/2 transitions, which is derived from

$$\frac{1}{\tau} = \frac{1}{\tau_1} + \frac{1}{\tau_2},$$

where τ_1 and τ_2 correspond to the radiative lifetimes of the transitions (2)1/2–$X^2\Sigma$+1/2 and (1)3/2–$X^2\Sigma$+1/2, respectively, and τ is the total radiative lifetime of $A^2\Pi$–$X^2\Sigma^+$. The results are also listed in Table 4. It can be seen that our calculated lifetimes for the $\nu = 0$ and 1 levels of $A^2\Pi$ state are 46.91 and 45.78 ns, while the experimental data are 43.6±3 and 44.4±4 ns,[46] respectively, and (1)3/2–$X^2\Sigma$+1/2 plays an important role in the observed transition $A^2\Pi$–$X^2\Sigma^+$. The (3)1/2–$X^2\Sigma$+1/2 transition has smaller lifetimes than the (2)1/2–$X^2\Sigma$+1/2 transition due to the fact that the former has larger TDMs values in the Franck–Condon region. The lifetimes of $A^2\Pi$–$X^2\Sigma^+$ are consistent with the reported results,[24] while the (3)1/2–$X^2\Sigma$+1/2 transition is far less than the $B'^2\Sigma^+$–$X^2\Sigma^+$ transition,[24] which may be the effect of SOC.

Table 4. Radiative lifetimes of the transitions from (2)1/2, (1)3/2 and (3)1/2 to the $X^2\Sigma$+1/2 state.

Transition	Radiative lifetimes (ns)		
	$\nu' = 0$	$\nu' = 1$	$\nu' = 2$
(2)1/2–$X^2\Sigma$+1/2	226.35	224.11	233.80
(1)3/2–$X^2\Sigma$+1/2	59.17	57.79	53.56
$A^2\Pi$–$X^2\Sigma^+$	46.91	45.78	43.58
Calc.[24]	46	47.3	49
Expt.[44]	43.6±3	44.4±4	-
(3)1/2–$X^2\Sigma$+1/2	75.73	74.38	73.31
Calc.[24]	126	127	135

In summary, the high-level relativistic MRCI+Q calculations on the ground and low-lying excited states of MgH radical have been performed. The PECs of five Λ-S states are plotted and the corresponding spectroscopic constants are derived, which are in good accordance with the experimental data. The PDMs of the ground state reach 0 a.u. at the internuclear distance 3.6 Å and the other excited states reach 0 a.u. at large distances. The SO matrix elements reveal the sharp changes for the electron configurations in the wave functions of $A^2\Pi$ and $B'^2\Sigma^+$ states at their avoided crossing point. The five Λ-S states split into ten Ω states and the (2)1/2 state produces double-well potential after taking the SOC effect into account. The transition properties of (2)1/2–$X^2\Sigma$+1/2, (1)3/2–$X^2\Sigma$+1/2 and (3)1/2–$X^2\Sigma$+1/2 are reported and the calculated lifetime of $A^2\Pi$–$X^2\Sigma^+$ is in good agreement with the measurements. The present study is expected to provide an accurate global picture of a manifold of electronic states of MgH, and thus reliable data to guide further experimental spectroscopic investigations.

References

[1] Sotirovski P 1972 *Astron. Astrophys. Suppl. Ser.* **6** 85
[2] Wallace L et al 1999 *Astrophys. J.* **524** 454
[3] Kirkpatrick J D 2005 *Annu. Rev. Astron. Astrophys.* **43** 195
[4] Boesgaard A M 1968 *Astrophys. J.* **154** 185
[5] Gay P L and Lambert D L 2000 *Astrophys. J.* **533** 260
[6] Watson W W and Rudnick P 1926 *Astrophys. J.* **63** 20
[7] Grundström B 1936 *Nature* **137** 108
[8] Turner L A and Harris W T 1937 *Phys. Rev.* **52** 626
[9] Pearse R W B 1929 *Proc. R. Soc.* A **122** 442
[10] Ziurys L M et al 1993 *Astrophys. J.* **402** L21
[11] Shayesteh A et al 2004 *J. Chem. Phys.* **120** 10002
[12] Bernath P F et al 1985 *Astrophys. J.* **298** 375
[13] Shayesteh A et al 2007 *J. Phys. Chem.* A **111** 12495
[14] Shayesteh A et al 2003 *J. Chem. Phys.* **118** 1158
[15] Leopold K R et al 1986 *J. Chem. Phys.* **84** 1935
[16] Lemoine B et al 1988 *J. Chem. Phys.* **89** 673
[17] Shayesteh A et al 2011 *J. Chem. Phys.* **135** 094308
[18] Saxon R P et al 1978 *J. Chem. Phys.* **69** 5301
[19] Weck P F et al 2003 *Astrophys. J.* **582** 1059
[20] Weck P F et al 2003 *Astrophys. J.* **584** 459
[21] Skory S et al 2003 *Astrophys. J. Suppl. Ser.* **148** 599
[22] Mestdagh J M 2009 *Chem. Phys. Lett.* **471** 22
[23] Guitou M et al 2010 *Chem. Phys. Lett.* **488** 145
[24] Mostafanejad M and Shayesteh A 2012 *Chem. Phys. Lett.* **551** 13
[25] Werner H J et al 2012 *MOLPRO: a package of ab initio programs*
[26] Le Roy R J 2007 *LEVEL 8. 0: A Computer Program for Solving the Radial Schrödinger Equation for Bound and Quasibound Levels* (University of Waterloo: Chemical Physics Research Report CP-663)
[27] Peterson K A and Dunning T H 2002 *J. Chem. Phys.* **117** 10548
[28] Woon D E and Dunning T H J 1993 *J. Chem. Phys.* **98** 1358
[29] Werner H J and Knowles P J 1985 *J. Chem. Phys.* **82** 5053
[30] Knowles P J and Werner H J 1985 *Chem. Phys. Lett.* **115** 259
[31] Werner H J and Knowles P J 1988 *J. Chem. Phys.* **89** 5803
[32] Knowles P J and Werner H J 1988 *Chem. Phys. Lett.* **145** 514
[33] Berning A et al 2000 *Mol. Phys.* **98** 1823
[34] Huber K P and Hertzberg G 1979 *Molecular Spectrum and Molecular Structure IV, Constants of Diatomic Molecules* (New York: Van Nostrand Reinhold)
[35] Wu D L et al 2015 *Chin. Phys.* B **24** 043401
[36] Wu D L et al 2015 *Spectrochim. Acta Part* A **150** 499
[37] Liang G Y et al 2016 *Spectrochim. Acta Part* A **156** 9
[38] Zhang X M et al 2014 *Chem. Phys.* **443** 142
[39] Liu Y F et al 2012 *Comput. Theor. Chem.* **991** 82
[40] Li Q N et al 2015 *Chin. Phys. Lett.* **32** 073103
[41] Moore C E 1971 *Atomic Energy Levels* (Washington: National Bureau of Standards)
[42] Zhang Y P et al 2004 *Phys. Rev. Lett.* **92** 203003
[43] Zhang Y P et al 2005 *Chin. Phys. Lett.* **22** 1114
[44] Okabe H 1978 *Photochemistry of Small Molecules* (New York: Wiley-Interscience)
[45] Wu D L et al 2016 *Spectrochim. Acta Part* A **161** 101
[46] Nedelec O and Dufayard J 1978 *J. Chem. Phys.* **69** 1833